Key Points:
- The magnitude of SYM-H is found to be enhanced under northward Z-component of interplanetary magnetic field conditions present during the 21 January 2005 storm
- A highly dense central plasma sheet played a key role in creating the anomalous plateau phase of SYM-H
- Space weather models need to account for the state of the magnetosphere to successfully reproduce all the features of the SYM-H index

Correspondence to:
D. Rout,
diptiprl89@gmail.com

The Growth of Ring Current/SYM-H Under Northward IMF B_z Conditions Present During the 21–22 January 2005 Geomagnetic Storm

Diptiranjan Rout[1,2] , S. Patra[3], S. Kumar[4] , D. Chakrabarty[5], G. D. Reeves[6], C. Stolle[7] , K. Pandey[8] , S. Chakraborty[9] , and E. A. Spencer[10]

[1]GFZ German Research Centre for Geosciences, Potsdam, Germany, [2]National Atmospheric Research Laboratory, Gadanki, India, [3]University of New Brunswick, Fredericton, NB, Canada, [4]Institute for Space-Earth Environmental Research, Nagoya University, Nagoya, Japan, [5]Physical Research Laboratory, Ahmedabad, India, [6]Los Alamos National Laboratory, Los Alamos, NM, USA, [7]Leibniz Institute of Atmospheric Physics at the University of Rostock, Kuhlüngsborn, Germany, [8]Department of Physics and Engineering Physics, ISAS, University of Saskatchewan, Saskatoon, SK, Canada, [9]Center for Space Science and Engineering Research Bradley Department of Electrical and Computer Engineering, Virginia Tech, Blacksburg, VA, USA, [10]Department of Electrical and Computer Engineering, University of South Alabama, Mobile, AL, USA

Abstract The total energy transfer from the solar wind to the magnetosphere is governed by the reconnection rate at the magnetosphere edges as the Z-component of interplanetary magnetic field (IMF B_z) turns southward. The geomagnetic storm on 21–22 January 2005 is considered to be anomalous as the SYM-H index that signifies the strength of ring current, decreases and had a sustained trough value of −101 nT lasting more than 6 hr under northward IMF B_z conditions. In this work, the standard WINDMI model is utilized to estimate the growth and decay of magnetospheric currents by using several solar wind-magnetosphere coupling functions. However, it is found that the WINDMI model driven by any of these coupling functions is not fully able to explain the decrease of SYM-H under northward IMF B_z. A dense plasma sheet along with signatures of a highly stretched magnetosphere was observed during this storm. The SYM-H variations during the entire duration of the storm were only reproduced after modifying the WINDMI model to account for the effects of the dense plasma sheet. The limitations of directly driven models relying purely on the solar wind parameters and not accounting for the state of the magnetosphere are highlighted by this work.

Plain Language Summary The transfer of energy from the solar wind to the Earth's magnetosphere works best when the Z-component of interplanetary magnetic field (IMF B_z) points southward. Generally, the southward IMF B_z drives the ring current whose strength is estimated by the Dst/SYM-H indices. The storm on 21 January 2005 is one of the rarest events as the Dst/SYM-H index kept decreasing for more than 6 hr and reached a very low value of −101 nT after IMF B_z turned northward. In this work, we have estimated the value of SYM-H by using various solar wind-magnetosphere coupling functions as input to the WINDMI model. However, none of these coupling functions could estimate the unexpected decrease of SYM-H index under the northward IMF B_z conditions. The plasma sheet was found to be highly dense during this event. The WINDMI model could successfully reproduce the SYM-H index by incorporating this change in plasma sheet density. This investigation clearly demonstrates that the state of the Earth's magnetosphere plays a crucial role in strengthening the magnetospheric currents. Based on these findings, we suggest that space weather models need to include both the conditions of solar wind and magnetosphere to get a better prediction of the strength of the ring current.

1. Introduction

The energy and mass transfer from the solar wind to the Magnetosphere-Ionosphere (MI) system depends on solar wind parameters and the state of the magnetosphere and ionosphere. A great many theories have been proposed to quantify these interactions (Borovsky, 2013; Gonzalez et al., 1994; Newell et al., 2007) most of which are based on the classical Dungey paradigm (Dungey, 1961). The largest energy reservoirs in the magnetosphere are the westward flowing ring current and the magnetotail current. The ring current gets energized during a geomagnetic storm when the z-component of the interplanetary magnetic field (IMF B_z) turns southward. The energy transfer from the solar wind is more effective when conditions suitable for magnetic reconnection are present on the

dayside magnetopause (Borovsky & Birn, 2014; Gonzalez & Tsurutani, 1987; Rostoker & Fälthammar, 1967; Tsurutani & Meng, 1972). The orientation of the IMF heavily controls the rate and location of reconnection. While the most effective reconnection happens under southward IMF B_z conditions, other solar wind parameters significantly affect it (Chakrabarty et al., 2017; Newell et al., 2007; Rout et al., 2017).

Magnetospheric dynamics are quite distinct when the IMF B_z is northward. The geoeffectiveness of the solar wind drops significantly under northward IMF conditions (Tsurutani & Gonzalez, 1995). Reconnection takes place at high latitudes leading to a four-cell convection pattern (Burke et al., 1979). Parameters like the solar wind, IMF B_y, geomagnetic dipole field, and the dipole tilt control the energy and mass transfer during northward IMF (Li et al., 2008; Reistad et al., 2019). Under extended periods of northward IMF B_z conditions the plasma sheet transforms into a cold dense plasma sheet (CDPS) (Sorathia et al., 2019; Taylor et al., 2008). Reconnection occurs at locations poleward of the cusp that lead to the capture of interplanetary flux tubes that sometimes contain filament material by the magnetosphere to create the CDPS (Kozyra et al., 2013; Li et al., 2008; Palmroth et al., 2006). This preconditioning which typically takes about 3 hr is known to lead to a stronger geomagnetic storm if the IMF B_z turns southward immediately after the period of northward IMF B_z (Wing et al., 2006). The development and recovery of most of the geomagnetic storms in recorded history can be explained by one or more of these simplified theories but there have also been a few reported events that were deemed "anomalous" since the storms were reported to have developed when no energy was being transferred from the solar wind, typically associated with a period of northward IMF B_z (Du et al., 2008; Kleimenova et al., 2015; Simi et al., 2012).

Echer et al. (2008) reported that during the solar cycle 23 (1996–2006), all intense geomagnetic storms (Dst ≤ -100) were found to occur under IMF B_z southward conditions. However, the storm on 21 January 2005 is the only reported event that had a main phase and extended peak lasting more than 6 hr under northward IMF Bz condition. A few researchers have analyzed the cause of this anomalous storm and modeled it using physics-based and empirical models (Dmitriev et al., 2014; Du et al., 2008; Kalegaev et al., 2015; Kozyra et al., 2014). Storage and delayed injection were provided as a plausible explanation for the enhanced $|SYM - H|$ during the northward IMF period by Du et al. (2008) and Kane (2012). Others have discussed the unaccounted contributions from additional solar wind parameters, magnetospheric and ionospheric currents (Dmitriev et al., 2014; Troshichev & Janzhura, 2012). The presence of a CDPS that enabled the extreme compression to energize particles adiabatically has also been suggested as a possible energization mechanism (Kozyra et al., 2013). However, none of these theories could properly explain the growth of $|SYM - H|$ under northward IMF B_z condition. Therefore, the fundamental question that needs to be answered is what could drive the ring current or contribute to the growth of $|SYM - H|$ during northward IMF B_z conditions when there is no direct energy input from the solar wind. In this study, we successfully reproduce all the features SYM-H measured during the 21 January 2005 storm by using the WINDMI model (Horton & Doxas, 1998; Patra et al., 2011; Spencer et al., 2007) driven by a few standard coupling functions. The results suggest that the strength of the SYM-H is not only controlled by the solar wind conditions but also depends on the state of the magnetosphere.

2. Event Overview

The coronal mass ejection that erupted on 20 January 2005 from the X7.1/3B solar flare in the northwestern quadrant of the solar disk (14°N, 61°W), caused a moderate geomagnetic storm on 21 January 2005 (Foullon et al., 2007). Figure 1 shows the solar wind parameters at the L1 point (in geocentric solar magnetospheric coordinate system) as measured by the Advance Composition Explorer (ACE) satellite. These have been shifted by 24 min to align with the geomagnetic signatures of arrival of the interplanetary shock. The strength of the geomagnetic storm during 21–22 January 2005 as signified by the geomagnetic indices is shown in the figure along with the magnetopause standoff distance (L_{mp} in R_E). This storm is mainly characterized by an interplanetary shock and a interplanetary discontinuity (indicated as S and D in red dashed lines, respectively). The interplanetary shock is observed by ACE at 16:48 UT that arrived at the magnetopause at ~17:12 UT on 21 January (marked with an S). An unusual double-discontinuity, characterized by a noncompressive density enhancement (Foullon et al., 2007), arrived ~1.5 hr later (at 18:43 UT) on 21 January, causing a second SI+ at 1900 UT (Du et al., 2008). This discontinuity is indicated by a vertical dotted red line labeled as "D." It can be seen that the solar wind parameters ($|B|$, solar wind density, and velocity) changed sharply at these times. The proton density (N) increased from 2–22 cc^{-1} during the arrival of the shock, S, and further increased to an unusually high value of 62 cc^{-1} due to the second SI+. The solar wind velocity increased from 565 to 900 km/s. The solar wind dynamic
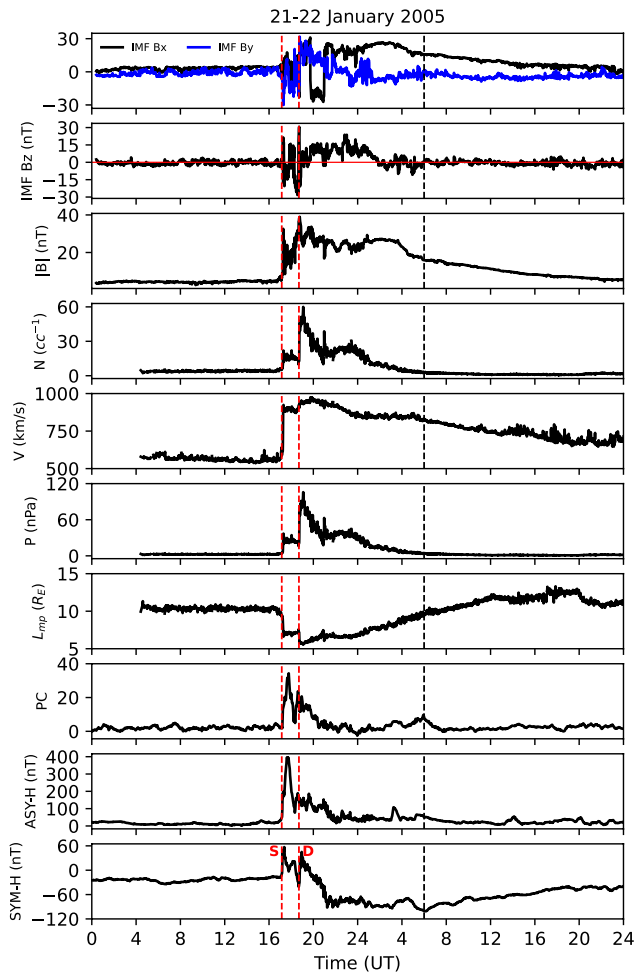
Figure 1. From top to bottom are X and Y components of IMF (IMF B_x and IMF B_y) in blue and black lines, north-south or Z component of IMF (IMF B_z in nT), total magnetic field intensity ($|B|$ in nT), solar wind proton density (N in cc^{-1}), solar wind velocity (V in km/s), solar wind dynamic pressure (P in nPa), variation of the magnetopause standoff distance (L_{mp} in R_E), polar cap index, ASY-H index in nT, and geomagnetic storm index (SYM-H in nT). The red dashed vertical are drawn to identify the two interplanetary shocks (SI + s).

pressure $\left(P = \frac{1}{2}\rho V^2 \right)$ increased from 2 to 35 nPa and then it increased to the significantly high value of 106 nPa due to the second SI+. Due to the high dynamic pressure, the magnetopause standoff distance was estimated to be significantly reduced from ∼10.3 R_E to 5.3 R_E based on the formula provided in Kivelson and Russell (1995). The subsolar magnetopause was continuously located inside geosynchronous orbit (∼6R_E) as a consequence of the strong compression during the initial and main phases of the storm. It is for the first time that the upstream solar wind was observed at geosynchronous orbit for almost 2 hr due to the extreme compression caused by the solar wind dynamic pressure (Dmitriev et al., 2014).

In response to the arrival of shock, the SYM-H increased from −17 to 55 nT. Approximately 1.5 hr later (at 18:43 UT) the second SI+ front arrived which led to a second increase in the SYM-H value. It is around this time that the IMF B_z turned northward, but surprisingly the storm's main phase continued to develop. In between, the IMF B_z turned southward within minutes of the arrival of the shock (SI+) at 17:20 UT, it briefly turned northward at 17:47 UT but turned southward again at 18:18 UT, and remained southward until a few minutes before the arrival of the second SI+ at 18:45 UT. The SYM-H reached its lowest value of −101 nT at 06:00 UT on 22 January. The IMF B_z was continuously northward from 19:40 UT, 21 January to 02:45 UT, 22 January 2005 except for a brief period lasting 7 min from 20:45 – 20:52 UT when it turned southward. During this minor excursion, the IMF B_z only dropped down to the value of around −5 nT. This small period of southward IMF B_z is not expected to provide enough energy to sustain the depressed SYM-H (Liu et al., 2018). Typically, when the IMF B_z turns northward the ring current starts to recover and this recovery is observed in the SYM-H values. But surprisingly during the period from 19:40 UT, 21 January–02:45 UT, 22 January 2005, the SYM-H index decreased to a value of around −90 nT by 21:30 UT and remained depressed afterward which is referred to as the "plateau" region. This is highly unusual and termed "anomalous" as reported by a few other studies (Bag et al., 2023; Du et al., 2008; Kozyra et al., 2013, 2014; McKenna-Lawlor et al., 2010). Additionally, the polar cap index, and the indicator of ring current asymmetry (ASY-H) were significantly high during the initial phase but dropped quickly during the main phase.

3. Results and Discussion

In order to explain the unusual decrease of the SYM-H, the low-order physics-based model of the magnetosphere-ionosphere system, WINDMI (Horton & Doxas, 1998; Spencer et al., 2007) is used. The WINDMI model is derived from the fluid plasma equations that give a system of eight ordinary differential equations driven by a potential derived from solar wind coupling functions. The eight equations of the model are given by:

$$L\frac{dI}{dt} = V_{sw}(t) - V + M\frac{dI_1}{dt} \tag{1}$$

$$C\frac{dV}{dt} = I - I_1 - I_{ps} - \Sigma V \tag{2}$$

$$\frac{3}{2}\frac{dp}{dt} = \frac{\Sigma V^2}{\Omega_{cps}} - u_0 p K_\parallel^{1/2}\Theta(u) - \frac{pV A_{eff}}{\Omega_{cps} B_{tr} L_y} - \frac{3p}{2\tau_E} \tag{3}$$

$$\frac{dK_\parallel}{dt} = I_{ps}V - \frac{K_\parallel}{\tau_\parallel} \tag{4}$$

$$L_I \frac{dI_1}{dt} = V - V_I + M\frac{dI}{dt} \tag{5}$$

$$C_I \frac{dV_I}{dt} = I_1 - I_2 - \Sigma_I V_I \tag{6}$$

$$L_2 \frac{dI_2}{dt} = V_I - \left(R_{\text{prc}} + R_{A2}\right)I_2 \tag{7}$$

$$\frac{dW_{\text{rc}}}{dt} = R_{\text{prc}}I_2^2 + \frac{pV A_{\text{eff}}}{B_{\text{tr}}L_y} - \frac{W_{\text{rc}}}{\tau_{\text{rc}}} \tag{8}$$

The model is driven by a potential field that is a function of the solar wind parameters (V_{sw}). The nonlinear equations of the model trace the flow of electromagnetic and mechanical energy through eight pairs of transfer terms. The remaining terms describe the loss of energy from the magnetosphere-ionosphere system through plasma injection, ionospheric losses and ring current energy losses. It should be noted that the current version of the model represents the state of the magnetosphere-ionospheric system more accurately under southward IMF conditions. The quiet time response of the WINDMI model is produced by driving it with a constant viscous voltage V_{visc}. During purely northward IMF B_z, dayside merging and high-latitude reconnections create the northward Bz (NBZ) currents system. The WINDMI model currently doesn't incorporate these or any potential plasma circulation due to viscous interactions. Though these effects are not expected to be sufficient to sustain the near −100 nT depression in SYM-H observed in the plateau phase of the storm. Nevertheless, these effects should be estimated to formulate a better understanding of any storm.

The 22 coefficients in the WINDMI differential equations are physical parameters of the magnetosphere-ionosphere system. The quantities L, C, Σ, L_1, C_I and Σ_I are the magnetospheric and ionospheric inductances, capacitances, and conductances respectively. A_{eff} is an effective aperture for particle injection into the ring current. The resistances in the partial ring current and region-2 current, I_2 are R_{prc} and R_{A2} respectively, and L_2 is the inductance of the region-2 current. The coefficient u_0 in Equation 3 is a heat flux limiting parameter. The energy confinement times for the central plasma sheet, parallel kinetic energy, and ring current energy are τ_E, τ_k, and τ_{rc} respectively. The effective width of the magnetosphere is L_y and the transition region magnetic field is given by B_{tr}. The pressure gradient-driven current is given by $I_{ps} = L_x(p/\mu_0)^{1/2}$, where L_x is the effective length of the magnetotail. The outputs of the model relevant to the current study are the magnetotail current (I), ring current energy (W_{rc}), in addition to all the magnetospheric field-aligned currents.

The solar wind-magnetosphere interaction is usually quantified by coupling functions. The earliest of these was the half-wave rectified motional electric field which proposed that the x-component of solar wind velocity (v_x) and the southward component of IMF $B_z(B_s)$ were the most important parameters (Burton et al., 1975). Additional coupling functions have been introduced that account for the effect of dynamic pressure (P), the perpendicular component of the magnetic field (B_T), and the clock angle ($\theta = \tan^{-1}(B_y/B_z)$), magnetic flux at the magnetopause (Φ_{mp}), magnetosonic mach number, plasma beta value, mass density of the solar wind upstream of the bow shock (ρ_o), and thermal pressure (P_{th}) (Borovsky, 2008; Newell et al., 2007; Siscoe et al., 2002). These coupling functions are combined with the effective thickness of the magnetosphere L_y^{eff} and a base viscous voltage V_{visc} to obtain the driving potential ($V_{sw} = V_{xxx}$) for the model. We have chosen five coupling functions for this study as defined below:

$$V_{rectified} = V_{visc} + v_x B_s^{IMF} L_y^{eff} \qquad \text{—Rectified} \tag{9}$$

$$V_{siscoe} = V_{visc} + 57.6 v_x B_T \sin^2(\theta/2) P^{-1/6} \qquad \text{—Siscoe} \tag{10}$$

$$V_{newell} = V_{visc} + v_x^{4/3} B_T^{2/3} \sin^{8/3}(\theta/2) \qquad \text{—Newell} \tag{11}$$

$$V_{newell-P} = V_{visc} + P^{1/2}\frac{d\Phi_{mp}}{dt} \qquad \text{—Newell-P} \tag{12}$$

$$V_{borovsky} = V_{visc} + f(v, B, P, \theta, \rho_o, P_{th}) \qquad \text{—Borovsky} \tag{13}$$

For detailed information on the coupling functions and their performance please refer to Spencer et al. (2011). The chosen coupling functions are normalized based on the method proposed by Spencer et al. (2011), so that only the qualitative differences introduced by each function are highlighted. The WINDMI model estimates
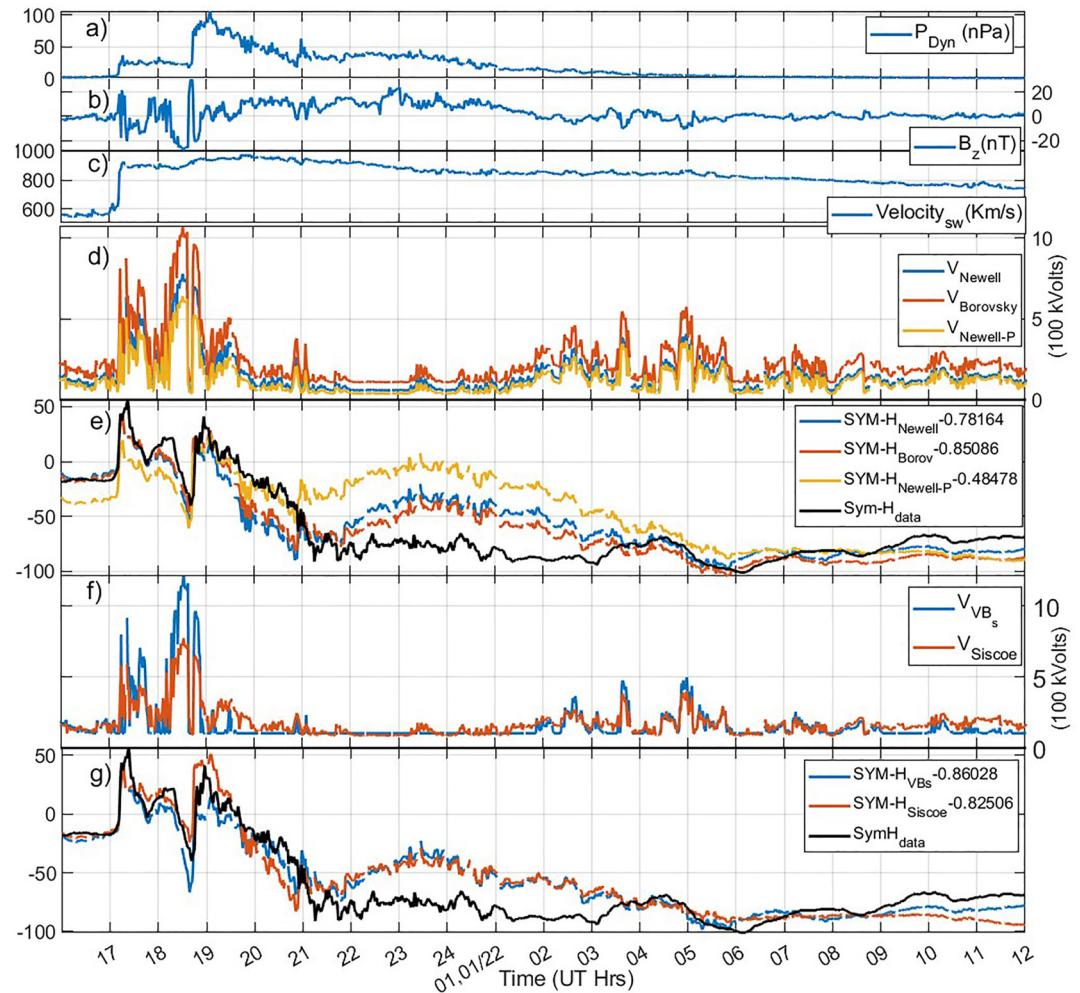
Figure 2. Top three panels (a)–(c) show the shifted solar wind dynamic pressure, z-component of magnetic field, and velocity measured at Advance Composition Explorer. The coupling functions (d and f), the modeled and measured SYM-H values (e and g) along with their correlation coefficients for the 21 January 2005 storm are shown in the bottom four panels.

the state of the magnetopshere-ionosphere system by optimizing the physical model parameters using a genetic algorithm (Patra et al., 2011). The contribution of the symmetric ring current energy ($W_r c$) to the SYM-H index is calculated using the Dessler-Parker-Sckopke relationship (Dessler & Parker, 1959; Sckopke, 1966) that relates the energy in the ring current with the magnetic perturbations at low latitudes on the surface of the Earth. The magnetic perturbation at low latitudes due to the magnetopause currents is estimated as $15.5\sqrt{P}$ based on the empirical relationship given by Burton et al. (1975) and O'Brien and McPherron (2000).

The relative contribution of the tail current to the SYM-H index has been estimated to range from 25% to 80% by various studies (Daglis et al., 2003; Gonzalez et al., 1994; Maltsev, 2004). Feldstein et al. (2005) estimated the magnetotail current contribution using Defence Meteorological Satellite Program satellite data and found nearly equal contributions from both the tail currents and the Chapman-Ferraro currents during a geomagnetic storm. It is well-established that the inner boundary location of the magnetotail current sheet influences the strength of magnetic perturbations observed on Earth's surface. To account for the uncertainty in the tail current contribution (I) to the SYM-H index, the WINDMI model, as described in Equation 1, incorporates a geometric factor (Patra et al., 2011). The estimated SYM-H value calculated by the WINDMI model for each coupling function is the sum of all three current contributions, as illustrated in Figure 2.

The best-fit results along with the normalized coupling function values are shown in Figures 2d–2g. During the initial and main phase of the storm until around 21:30 UT, almost all the coupling functions are able to provide acceptable fits. The rectified E-field and Borovsky's coupling functions provide the best fits with correlation

values of 0.86 and 0.85 respectively as shown in the panels showing the modeled SYM-H values in Figure 2. The initial decrease of the SYM-H after the northward turning of IMF B_z around 18:43 UT can be correctly estimated due to the reduction in magnetopause currents and the delayed response of the currents. From 21:30 UT onwards until 04 UT in the plateau phase the model tends to overpredict the SYM-H values.

The consistent overestimation by the WINDMI model from 21:30– 04:00 UT is due to the fact that none of the coupling functions predict any substantial energy injection in this period. This suggests that directly driven mechanisms even after accounting for other solar wind variables as suggested by Kuznetsova and Laptukhov (2011), and Troshichev and Janzhura (2012), might not have been the dominant contributor to the ring current during this phase. A delayed rise of the ring current, which can be from 0 to 8 hr, and slow decay was suggested as a likely cause by Kane (2012), and Gonzalez and Echer (2005). The WINDMI model successfully reproduced the delayed decrease in SYM-H, and predicts a slow decay of the ring current with a relatively high time constant of ∼10 hr. The inability of the model to fit the plateau suggests either additional ring current energization mechanisms might have been present or other current sources contributed to the steady SYM-H. It is also likely that the simple expression of pressure correction used to account for the effects of Chapman-Ferraro currents doesn't hold under all the stages of the storm. Siscoe et al. (2005) found diminished contributions of the ram pressure to SYM-H index during storms. In this work, we are exploring if the unique conditions present during the storm might have affected the state of the ring and tail currents.

Du et al. (2008) reported that the magnetic field stretching angle was close to zero during the initial phase which signifies a highly distorted magnetosphere and an earthward location of the tail current that suggests a significant contribution from the tail current to the low latitude magnetic disturbance. Empirical and magnetohydrodynamics models validated using in-situ and energetic neutral atoms observations have been used to model the various currents' contributions to SYM-H (Dmitriev et al., 2014; Kozyra et al., 2014; McKenna-Lawlor et al., 2010). From these studies, it was inferred that the currents like the field-aligned currents, tail currents, and partial ring current were the dominant contributors during the main and early recovery phase of the storm while the symmetric ring current became dominant after 00:45 UT on 22 January.

Kozyra et al. (2014) reported observations of an intensified auroral oval, isotropic boundary (b2i) at lower latitudes, and the ring current precipitation zones that are evidence for the magnetotail stretching by field line curvature scattering. Kozyra et al. (2013) claim that the 21 January 2005 event was the first and only instance where a strong stretching was observed due to the formation of a dense plasma sheet derived from dense solar filament material. Based on the evidence, it is reasonable to assume that the tail current remained elevated and contributed to the SYM-H index during the main phase. The plasma sheet capacitance parameter C in the WINDMI model Equation 2 is a function of the plasma sheet density. The capacitance value can be determined using the following expression (Spencer, 2006):

$$C \approx \frac{\pi \rho_m L_x L_z}{B_{x0} B_z L_y}$$

(14)

where ρ_m is the plasma sheet density, L_x and L_y are the length and width of the geotail while L_z is the half-width of the plasma sheet. B_{x0} is the magnetic field at $x = 0$ and B_z is constant.

Figure 3a shows the plasma sheet density as measured by the Los Alamos National Laboratory Magnetospheric Plasma Analyzers (LANL-MPA). Observations from all the satellites (LANL-95, LANL-84, LANL-97A, LANL-01A, and LANL-02A) during 20:00–04:00 magnetic local time window are plotted at a given UT. The density increases by almost 6–10 times after the second impulse (SI+). To reflect this abrupt increase in density we chose a step profile for the plasma sheet capacitance changing from ∼70,000 to 560,000 F. The contribution of the various currents to the SYM-H index (SYM-H$_{windmi}$) as estimated by the WINDMI model driven by the rectified function and density-dependent Capacitance is shown in Figure 3. The breakdown of currents estimated by the standard model driven by the rectified function as shown earlier in Figure 2 is also shown with dashed lines.

The modified model estimates a much more accurate value for SYM-H as compared with the standard model in the plateau region. The modified model estimates an even slower ring current (SYM-H$_{rc}$) decay with a time constant of ∼13 hr. The fast dynamics in the initial and main phases are the result of the Chapman-Ferraro (magnetopause) currents (D_{mp}) and the tail current (SYM-H$_{tail}$). In the plateau phase the slowly decaying ring current, the still elevated tail current, and the magnetopause current combine to create a near-constant magnetic disturbance that matches with the observed records of the SYM-H index (SYM-H$_{data}$). The standard model predicts a gradual decay of the ring current but estimates a quick rise, albeit with a relatively modest enhancement, for
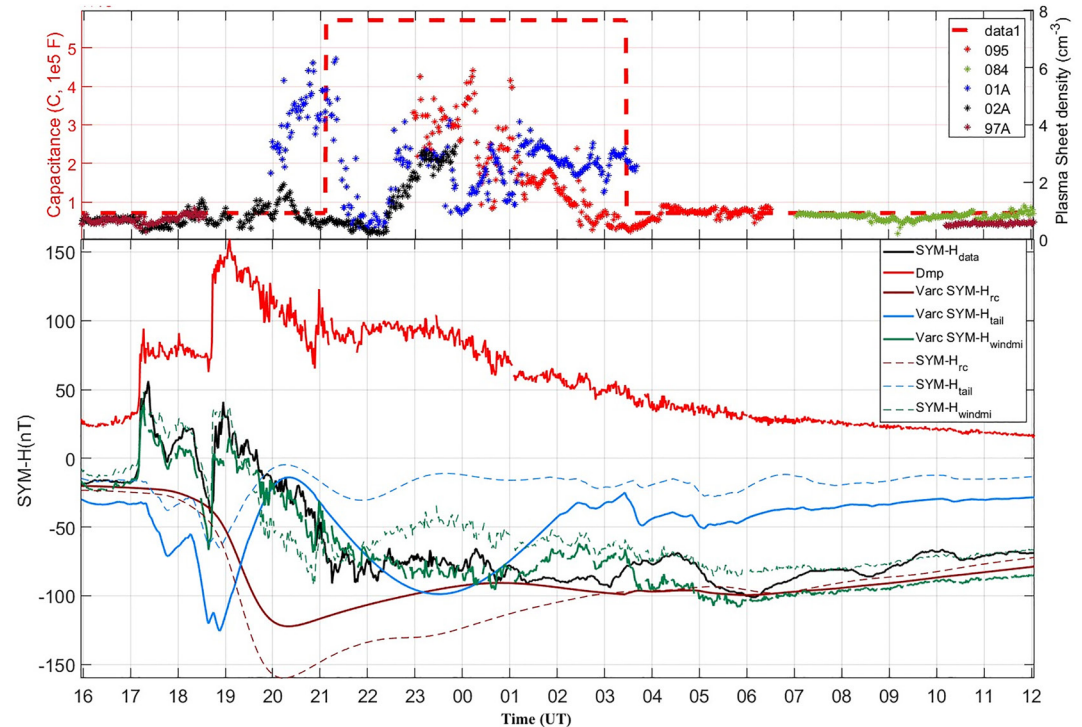
Figure 3. (a) Variation of plasma sheet density measured by different LANL satellites along with the modified plasma sheet capacitance used in the WINDMI model. (b) The measured and modeled SYM-H, magnetospheric currents for the 21 January 2005 storm as estimated by the WINDMI model with standard (dotted lines) and plasma sheet-dependent capacitance (solid lines) driven by the rectified VBs input (see text for details). The magnetopause current (Dmp) is estimated empirically.

the tail current. This is the expected response of the tail current in the standard WINDMI model as it is highly correlated with the input and has faster response times. Two different states of the magnetosphere-ionosphere system are estimated by the optimization algorithm in order to reproduce the observed SYM-H index. The change in capacitance mimicking the high plasma sheet density led to the change in the time constant of the tail current that resulted in elevated levels of the tail current.

This breakdown of the current contributions to SYM-H also highlights the fallacies in using commonly used terminologies like initial, main, and recovery phases of the storm based on just the SYM-H index. It is clear that the storm's main phase starts much earlier coinciding with the period of negative IMF B_z. The apparent growth of the storm main phase and the inflection point in SYM-H at 21:15 UT is in fact due to the recovery of the CF-current (magnetopause) after the second impulse at 19:20 UT. The magnetic perturbation caused by the magnetopause current (D_{mp}) peaked at 19:20 UT reaching a value of 155 nT and quickly fell down to a value around 80 nT from 21:15 UT till 24 UT. Hence one should be careful in interpreting and trying to model the ring current based purely on the basis of SYM-H.

The occurrence of dense plasma sheet and its role in magnetotail dynamics and ring current intensity was discussed in detail by Borovsky et al. (1997). They suggested three main sources for the higher density: the outer plasmasphere, high density solar wind, and ionospheric outflow. A CDPS usually forms under extended periods of northward IMF B_z (Borovsky & Denton, 2010; Denton & Borovsky, 2012). This dense material can be injected to the inner magnetosphere either by sudden southward IMF or a very strong compression (Thomsen et al., 2003). The long lifetime of the ring current was probably due to particle injection into the inner magnetosphere where the drift times are longer (Dmitriev et al., 2014). The formation of a warm and later CDPS within 1 Hr after impact of the second pressure pulse and under northward IMF conditions was reported by Kozyra et al. (2013) during the 21–22 January 2005 storm. They claim that the high densities were driven by the dense solar filament material that produced strong diamagnetic stretching despite low levels of magnetic activity. Du et al. (2008) suggested that energy was initially stored in the tail due to a previous southward IMF B_z period albeit small and then later injected into the ring current leading to the decrease of SYM-H. Although no clear physical mechanism
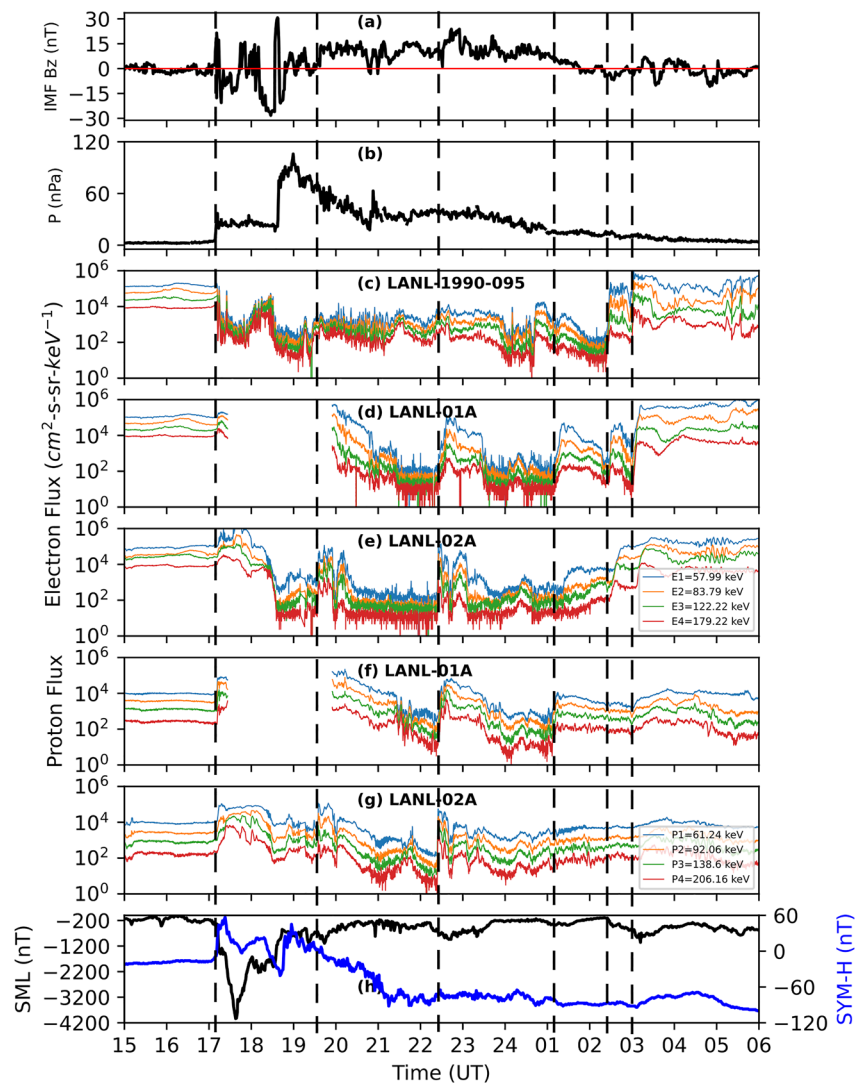
Figure 4. Variations in (a) IMF B_z, (b) Solar wind pressure, electron flux measured at geosynchronous orbit by (c) LANL-1990-095, (d) LANL-01A, (e) LANL-02A satellites, and proton flux measured by (f) LANL-01A, (g) LANL-02A satellites (h) SML and SYM-H indices. The black dashed lines are marked to show the time when the dispersionless-like injections are observed.

for this was provided, the creation of a dense plasma sheet followed by compression-led injection and substorms could possibly provide the additional source needed.

Figure 4 shows the variations of (a) IMF B_z, (b) solar wind pressure (P), electron flux measured at geosynchronous orbit by (c) LANL-1990-095, (d) LANL-01A, (e) LANL-02A satellites and proton flux measured by (f) LANL-01A, (g) LANL-02A satellites (h) SuperMAG westward AE index (SML), and SYM-H indices during 15:00 UT, 21 Januray-06:00 UT, 22 January. The dashed lines are marked to show the time when dispersionless-like injection of energetic particles at geosynchronous orbit is observed. These satellites were on the night side when the particle enhancements were observed. There are six dispersionless-like injections observed during this event which are also correlated with sharp reductions in SML index. The first substorm was observed by LANL-02A at 17:12 UT due to the arrival of the shock where the SML index is reduced to −4,418 nT, indicating an intensification of the westward auroral electrojet. This is considered as a shock-induced supersubstorm by Hajra and Tsurutani (2018). The SML attained a peak value of −4,418 nT at ∼17:38 UT and then started recovery. The SML index reached the pre-substorm level at ∼18:50, indicating the end of supersubstorm. It is to be noted that the substorm expansion phase continued for ∼21 min and the duration of the entire

supersubstorm event was ∼1 hr 40 min from the onset to end of the substorm (Hajra & Tsurutani, 2018). Recently, Tsurutani and Hajra (2023) studied various shock-induced supersubstorms where they found the supersubstorms occur in the main phase of an intense geomagnetic storm. It is observed that supersubstorm events occur simultaneously with concurrent magnetic storms and concluded that the supersubstorm event and the magnetic storm are closely related, if not the same thing. However, in the present investigation, the supersubstorm only lasts for 1 hr 40 min whereas, the main phase of the storm continued for more than 10 hr after the supersubstorm. This indicates that the supersubstorm did not play a significant role in the decrease of the SYM-H and had a negligible effect during the plateau region.

It is important to note that three (second, third, and fourth) dispersionless-like injections are observed under predominantly northward IMF B_z conditions although the fluxes are relatively low to the quiet time level. It can be seen that the solar wind pressure is high but not changing much during this time. The high solar wind pressure leads to a compressed magnetosphere that can lead to higher losses as the drifting particles might encounter the magnetopause and drift out (West et al., 1972). Alternatively, the possibility of the LANL satellites being on higher L-shells can not be ruled out since the magnetosphere is highly stretched. That can also result in lower flux measurements. These substorm-like signatures could then be just signatures of relaxation of the magnetosphere (Kozyra et al., 2013). The presence of a stretched magnetotail sustained by a high tail current and dense plasma sheet during the plateau phase of the storm possibly led to the anomalous SYM-H. The counterbalancing contributions from ring current, tail current, magnetopause current and the current wedge formed along with the long lifetimes of the ring current particles during the northward IMF B_z periods might have created conditions for the plateau observed in the SYM-H index (Lopez et al., 2015; Ohtani et al., 2001).

4. Summary

To summarize, in the present investigation, a moderate geomagnetic storm with a minimum SYM-H value of −110 nT that occurred on 21 January 2005 was unusually found to develop under northward IMF B_z conditions. The WINDMI model was used to understand the energization process of the ring current and other currents in the magnetosphere-ionosphere system by considering various coupling functions as input. It is found that the WINDMI fits that used the coupling function of Borovsky and rectified motional electric field as input gave the best correlations with the observed SYM-H. However, it is to be noted that none of the coupling functions could drive currents in the WINDMI model to reproduce the exact variation of SYM-H in the plateau phase. A highly dense plasma sheet was present during the plateau phase of the storm. This coincided with a highly stretched magnetosphere, as indicated by the isotropic boundary, suggesting a sustained high tail current with the inner edge of the tail closer to Earth. Multiple substorm-like signatures were found to be present during the northward IMF B_z conditions in the main phase of the storm that caused magnetic perturbations globally.

The WINDMI model was enhanced to include the contribution of plasma sheet density that allowed the WINDMI model to successfully reproduce all the features of the storm. The model estimates a slowly decaying ring current and a sustained tail current in the plateau phase. The long lifetime of the ring current was probably due to particle injection into the inner magnetosphere where the drift times are longer. A combination of the highly dense plasma sheet, long decay times of the ring current particles, and the elevated levels of the magnetopause currents likely caused the apparent growth, plateau, and extremely long recovery of the SYM-H index. Additionally, the potential non-linear contribution of the magnetopause currents and time-varying ring current decay rates can not be disregarded. The energy transfer from the solar wind to the magnetosphere-ionosphere system is the key to comprehending and predicting space weather. This study highlights the importance of correctly accounting for the state of the magnetosphere in successfully modeling currents during a geomagnetic storm.

Data Availability Statement

The geomagnetic indices (SYM-H and AL) and solar wind data are obtained from the GSFC/SPDF OMNIWeb (Papitashvili & King, 2020). The solar wind data is obtained from the ACE SWEPAM instrument (https://izw1.caltech.edu/ACE/ASC/level2/lvl2DATA_MAG-SWEPAM.html). The WINDMI model v.1 can be run for free at the Community coordinated modeling center (CCMC) (https://ccmc.gsfc.nasa.gov/models/WINDMI~1.0). The windmi model and the data used in this study are available in a Zenodo repository (Rout et al., 2023). The database contains the LANL particle measurements, IMF, and Solar wind records for the storm duration. See the Zenodo record for more description of the model used and data sets.

References

Bag, T., Rout, D., Ogawa, Y., & Singh, V. (2023). Thermospheric no cooling during an unusual geomagnetic storm of 21-22 January 2005: A comparative study between TIMED/SABER measurements and TIEGCM simulations. *Atmosphere*, *14*(3), 556. https://doi.org/10.3390/atmos14030556

Borovsky, J. E. (2008). The rudiments of a theory of solar wind/magnetosphere coupling derived from first principles. *Journal of Geophysical Research*, *113*(A8), A08228. https://doi.org/10.1029/2007ja012646

Borovsky, J. E. (2013). Physical improvements to the solar wind reconnection control function for the Earth's magnetosphere. *Journal of Geophysical Research: Space Physics*, *118*(5), 2113–2121. https://doi.org/10.1002/jgra.50110

Borovsky, J. E., & Birn, J. (2014). The solar wind electric field does not control the dayside reconnection rate. *Journal of Geophysical Research: Space Physics*, *119*(2), 751–760. https://doi.org/10.1002/2013ja019193

Borovsky, J. E., & Denton, M. H. (2010). Magnetic field at geosynchronous orbit during high-speed stream-driven storms: Connections to the solar wind, the plasma sheet, and the outer electron radiation belt. *Journal of Geophysical Research*, *115*(A8), A08217. https://doi.org/10.1029/2009ja015116

Borovsky, J. E., Thomsen, M. F., & McComas, D. J. (1997). The superdense plasma sheet: Plasmaspheric origin, solar wind origin, or ionospheric origin? *Journal of Geophysical Research*, *102*(A10), 22089–22097. https://doi.org/10.1029/97ja02469

Burke, W. J., Kelley, M. C., Sagalyn, R. C., Smiddy, M., & Lai, S. T. (1979). Polar cap electric field structures with a northward interplanetary magnetic field. *Geophysical Research Letters*, *6*(1), 21–24. https://doi.org/10.1029/GL006i001p00021

Burton, R., McPherron, R., & Russell, C. (1975). An empirical relationship between interplanetary conditions and Dst. *Journal of Geophysical Research*, *80*(31), 4204–4214. https://doi.org/10.1029/ja080i031p04204

Chakrabarty, D., Hui, D., Rout, D., Sekar, R., Bhattacharyya, A., Reeves, G. D., & Ruohoniemi, J. M. (2017). Role of IMF B_y in the prompt electric field disturbances over equatorial ionosphere during a space weather event. *Journal of Geophysical Research: Space Physics*, *122*(2), 2574–2588. https://doi.org/10.1002/2016JA022781

Daglis, I., Kozyra, J., Kamide, Y., Vassiliadis, D., Sharma, A., Liemohn, M., et al. (2003). Intense space storms: Critical issues and open disputes. *Journal of Geophysical Research*, *108*(A5), 1208. https://doi.org/10.1029/2002ja009722

Denton, M., & Borovsky, J. (2012). Magnetosphere response to high-speed solar wind streams: A comparison of weak and strong driving and the importance of extended periods of fast solar wind. *Journal of Geophysical Research*, *117*(A9), A00L05. https://doi.org/10.1029/2011ja017124

Dessler, A., & Parker, E. N. (1959). Hydromagnetic theory of geomagnetic storms. *Journal of Geophysical Research*, *64*(12), 2239–2252. https://doi.org/10.1029/jz064i012p02239

Dmitriev, A. V., Suvorova, A. V., Chao, J.-K., Wang, C. B., Rastaetter, L., Panasyuk, M. I., et al. (2014). Anomalous dynamics of the extremely compressed magnetosphere during 21 January 2005 magnetic storm. *Journal of Geophysical Research: Space Physics*, *119*(2), 877–896. https://doi.org/10.1002/2013JA019534

Du, A., Tsurutani, B., & Sun, W. (2008). Anomalous geomagnetic storm of 21–22 January 2005: A storm main phase during northward IMFS. *Journal of Geophysical Research*, *113*(A10), A10214. https://doi.org/10.1029/2008ja013284

Dungey, J. W. (1961). Interplanetary magnetic field and the auroral zones. *Physical Review Letters*, *6*(2), 47–48. https://doi.org/10.1103/physrevlett.6.47

Echer, E., Gonzalez, W. D., Tsurutani, B. T., & Gonzalez, A. L. C. (2008). Interplanetary conditions causing intense geomagnetic storms (Dst <= −100 nT) during solar cycle 23 (1996–2006). *Journal of Geophysical Research*, *113*(A5), A05221. https://doi.org/10.1029/2007JA012744

Feldstein, Y. I., Levitin, A., Kozyra, J., Tsurutani, B., Prigancova, A., Alperovich, L., et al. (2005). Self-consistent modeling of the large-scale distortions in the geomagnetic field during the 24–27 September 1998 major magnetic storm. *Journal of Geophysical Research*, *110*(A11), A11214. https://doi.org/10.1029/2004ja010584

Foullon, C., Owen, C. J., Dasso, S., Green, L. M., Dandouras, I., Elliott, H. A., et al. (2007). Multi-spacecraft study of the 21 January 2005 ICME. Evidence of current sheet substructure near the periphery of a strongly expanding, fast magnetic cloud. *Solar Physics*, *244*(1–2), 139–165. https://doi.org/10.1007/s11207-007-0355-y

Gonzalez, W., & Echer, E. (2005). A study on the peak Dst and peak negative Bz relationship during intense geomagnetic storms. *Geophysical Research Letters*, *32*(18), L18103. https://doi.org/10.1029/2005gl023486

Gonzalez, W., Joselyn, J.-A., Kamide, Y., Kroehl, H. W., Rostoker, G., Tsurutani, B. T., & Vasyliunas, V. (1994). What is a geomagnetic storm? *Journal of Geophysical Research*, *99*(A4), 5771–5792. https://doi.org/10.1029/93ja02867

Gonzalez, W. D., & Tsurutani, B. T. (1987). Criteria of interplanetary parameters causing intense magnetic storms ($D_{st} < −100$ nT). *Planetary and Space Science*, *35*(9), 1101–1109. https://doi.org/10.1016/0032-0633(87)90015-8

Hajra, R., & Tsurutani, B. T. (2018). Interplanetary shocks inducing magnetospheric supersubstorms (SML < −2500 nT): Unusual auroral morphologies and energy flow. *The Astrophysical Journal*, *858*(2), 123. https://doi.org/10.3847/1538-4357/aabaed

Horton, W., & Doxas, I. (1998). A low-dimensional dynamical model for the solar wind driven geotail-ionosphere system. *Journal of Geophysical Research*, *103*(A3), 4561–4572. https://doi.org/10.1029/97ja02417

Kalegaev, V., Vlasova, N., & Peng, Z. (2015). Dynamics of the magnetosphere during geomagnetic storms on January 21–22, 2005 and December 14–15, 2006. *Cosmic Research*, *53*(2), 98–110. https://doi.org/10.1134/s0010952515020033

Kane, R. (2012). Interplanetary and geomagnetic parameters during January 16–26, 2005. *Planetary and Space Science*, *62*(1), 97–99. https://doi.org/10.1016/j.pss.2011.12.011

Kivelson, M. G., & Russell, C. T. (1995). Introduction to space physics.

Kleimenova, N., Gromova, L., Dremukhina, L., Levitin, A., Zelinsky, N., & Gromov, S. (2015). High-latitude geomagnetic effects of the main phase of the geomagnetic storm of November 24, 2001 with the northern direction of IMF. *Geomagnetism and Aeronomy*, *55*(2), 174–184. https://doi.org/10.1134/s0016793215020097

Kozyra, J. U., Liemohn, M. W., Cattell, C., De Zeeuw, D., Escoubet, C. P., Evans, D. S., et al. (2014). Solar filament impact on 21 January 2005: Geospace consequences. *Journal of Geophysical Research: Space Physics*, *119*(7), 5401–5448. https://doi.org/10.1002/2013JA019748

Kozyra, J. U., Manchester, W. B., Escoubet, C. P., Lepri, S. T., Liemohn, M. W., Gonzalez, W. D., et al. (2013). Earth's collision with a solar filament on 21 January 2005: Overview. *Journal of Geophysical Research: Space Physics*, *118*(10), 5967–5978. https://doi.org/10.1002/jgra.50567

Kuznetsova, T., & Laptukhov, A. (2011). Contribution of geometry of interaction between interplanetary and terrestrial magnetic fields into global magnetospheric state and geomagnetic activity. *Advances in Space Research*, *47*(6), 978–990. https://doi.org/10.1016/j.asr.2010.11.022

Li, W., Raeder, J., Thomsen, M. F., & Lavraud, B. (2008). Solar wind plasma entry into the magnetosphere under northward IMF conditions. *Journal of Geophysical Research*, *113*(A4), A04204. https://doi.org/10.1029/2007ja012604

Liu, J., Wang, W., Zhang, B., Huang, C., & Lin, D. (2018). Temporal variation of solar wind in controlling solar wind-magnetosphere-ionosphere energy budget. *Journal of Geophysical Research: Space Physics*, *123*(7), 5862–5869. https://doi.org/10.1029/2017ja025154

Lopez, R., Gonzalez, W., Vasyliūnas, V., Richardson, I., Cid, C., Echer, E., et al. (2015). Decrease in SYM-H during a storm main phase without evidence of a ring current injection. *Journal of Atmospheric and Solar-Terrestrial Physics*, *134*, 118–129. https://doi.org/10.1016/j.jastp.2015.09.016

Maltsev, Y. P. (2004). Points of controversy in the study of magnetic storms. *Space Science Reviews*, *110*(3–4), 227–267. https://doi.org/10.1023/b:spac.0000023410.77752.30

McKenna-Lawlor, S., Li, L., Dandouras, I., Brandt, P. C., Zheng, Y., Barabash, S., et al. (2010). Moderate geomagnetic storm (21–22 January 2005) triggered by an outstanding coronal mass ejection viewed via energetic neutral atoms. *Journal of Geophysical Research*, *115*(A8), A08213. https://doi.org/10.1029/2009JA014663

Newell, P., Sotirelis, T., Liou, K., Meng, C.-I., & Rich, F. (2007). A nearly universal solar wind-magnetosphere coupling function inferred from 10 magnetospheric state variables. *Journal of Geophysical Research*, *112*(A1), A01206. https://doi.org/10.1029/2006ja012015

O'Brien, T. P., & McPherron, R. L. (2000). Forecasting the ring current index Dst in real time. *Journal of Atmospheric and Solar-Terrestrial Physics*, *62*(14), 1295–1299. https://doi.org/10.1016/s1364-6826(00)00072-9

Ohtani, S., Nosé, M., Rostoker, G., Singer, H., Lui, A., & Nakamura, M. (2001). Storm-substorm relationship: Contribution of the tail current to Dst. *Journal of Geophysical Research*, *106*(A10), 21199–21209. https://doi.org/10.1029/2000ja000400

Palmroth, M., Laitinen, T., & Pulkkinen, T. (2006). Magnetopause energy and mass transfer: Results from a global MHD simulation. In *Annales geophysicae* (Vol. 24, pp. 3467–3480).

Papitashvili, N. E., & King, J. H. (2020). Omni 1-min data set [Dataset]. NASA Space Physics Data Facility. https://doi.org/10.48322/45bb-8792

Patra, S., Spencer, E., Horton, W., & Sojka, J. (2011). Study of Dst/ring current recovery times using the WINDMI model. *Journal of Geophysical Research*, *116*(A2), A02212. https://doi.org/10.1029/2010ja015824

Reistad, J. P., Laundal, K. M., Østgaard, N., Ohma, A., Thomas, E. G., Haaland, S., et al. (2019). Separation and quantification of ionospheric convection sources: 2. The dipole tilt angle influence on reverse convection cells during northward IMF. *Journal of Geophysical Research: Space Physics*, *124*(7), 6182–6194. https://doi.org/10.1029/2019ja026641

Rostoker, G., & Fälthammar, C. G. (1967). Relationship between changes in the interplanetary magnetic field and variations in the magnetic field at the Earth's surface. *Journal of Geophysical Research*, *72*(23), 5853–5863. https://doi.org/10.1029/JZ072i023p05853

Rout, D., Chakrabarty, D., Janardhan, P., Sekar, R., Maniya, V., & Pandey, K. (2017). Solar wind flow angle and geoeffectiveness of corotating interaction regions: First results. *Geophysical Research Letters*, *44*(10), 4532–4539. https://doi.org/10.1002/2017GL073038

Rout, D., Patra, S., Kumar, S., Chakrabarty, D., Reeves, G., Stolle, C., et al. (2023). Database for "the growth of ring current/sym-h under northward IMF B_z conditions present during the 21-22 January 2005 geomagnetic storm" in Space Weather [Dataset]. Zenodo. https://doi.org/10.5281/zenodo.8193127

Sckopke, N. (1966). A general relation between the energy of trapped particles and the disturbance field near the Earth. *Journal of Geophysical Research*, *71*(13), 3125–3130. https://doi.org/10.1029/jz071i013p03125

Simi, K., Thampi, S. V., Chakrabarty, D., Pathan, B., Prabhakaran Nayar, S., & Kumar Pant, T. (2012). Extreme changes in the equatorial electrojet under the influence of interplanetary electric field and the associated modification in the low-latitude f region plasma distribution. *Journal of Geophysical Research*, *117*(A3), A03331. https://doi.org/10.1029/2011ja017328

Siscoe, G., Erickson, G., Sonnerup, B. Ö., Maynard, N., Schoendorf, J., Siebert, K., et al. (2002). Hill model of transpolar potential saturation: Comparisons with MHD simulations. *Journal of Geophysical Research*, *107*(A6), SMP–8.

Siscoe, G., McPherron, R., & Jordanova, V. (2005). Diminished contribution of ram pressure to Dst during magnetic storms. *Journal of Geophysical Research*, *110*(A12), A12227. https://doi.org/10.1029/2005ja011120

Sorathia, K., Merkin, V., Ukhorskiy, A., Allen, R., Nykyri, K., & Wing, S. (2019). Solar wind ion entry into the magnetosphere during northward IMF. *Journal of Geophysical Research: Space Physics*, *124*(7), 5461–5481. https://doi.org/10.1029/2019ja026728

Spencer, E. (2006). *Analysis of geomagnetic storms and substorms with the WINDMI model*. The University of Texas at Austin.

Spencer, E., Horton, W., Mays, M., Doxas, I., & Kozyra, J. (2007). Analysis of the 3–7 October 2000 and 15–24 April 2002 geomagnetic storms with an optimized nonlinear dynamical model. *Journal of Geophysical Research*, *112*(A4), A04S90. https://doi.org/10.1029/2006ja012019

Spencer, E., Kasturi, P., Patra, S., Horton, W., & Mays, M. (2011). Influence of solar wind–magnetosphere coupling functions on the Dst index. *Journal of Geophysical Research*, *116*(A12), A12235. https://doi.org/10.1029/2011ja016780

Taylor, M., Lavraud, B., Escoubet, C., Milan, S., Nykyri, K., Dunlop, M., et al. (2008). The plasma sheet and boundary layers under northward IMF: A multi-point and multi-instrument perspective. *Advances in Space Research*, *41*(10), 1619–1629. https://doi.org/10.1016/j.asr.2007.10.013

Thomsen, M., Borovsky, J., Skoug, R., & Smith, C. (2003). Delivery of cold, dense plasma sheet material into the near-Earth region. *Journal of Geophysical Research*, *108*(A4), 1151. https://doi.org/10.1029/2002ja009544

Troshichev, O., & Janzhura, A. (2012). Magnetic disturbances developing under conditions of northward IMF. In *Space weather monitoring by ground-based means* (pp. 219–230). Springer.

Tsurutani, B. T., & Gonzalez, W. D. (1995). The efficiency of "viscous interaction" between the solar wind and the magnetosphere during intense northward IMF events. *Geophysical Research Letters*, *22*(6), 663–666. https://doi.org/10.1029/95GL00205

Tsurutani, B. T., & Hajra, R. (2023). Energetics of shock-triggered supersubstorms (SML < −2500 nT). *The Astrophysical Journal*, *946*(1), 17. https://doi.org/10.3847/1538-4357/acb143

Tsurutani, B. T., & Meng, C.-I. (1972). Interplanetary magnetic-field variations and substorm activity. *Journal of Geophysical Research*, *77*(16), 2964–2970. https://doi.org/10.1029/JA077i016p02964

West, H. I., Buck, R. M., & Walton, J. R. (1972). Shadowing of electron azimuthal-drift motions near the noon magnetopause. *Nature; Physical Science*, *240*(97), 6–7. https://doi.org/10.1038/physci240006a0

Wing, S., Johnson, J. R., & Fujimoto, M. (2006). Timescale for the formation of the cold-dense plasma sheet: A case study. *Geophysical Research Letters*, *33*(23), L23106. https://doi.org/10.1029/2006gl027110